Supercritical Transition in Plane Channel Flow with Spatially Periodic Perturbations

Michael F. Schatz, Randall P. Tagg, [a] and Harry L. Swinney

Center for Nonlinear Dynamics and Department of Physics, The University of Texas, Austin, Texas 78712

Paul F. Fischer [b] and Anthony T. Patera

Department of Mechanical Engineering, Massachusetts Institute of Technology, Cambridge, Massachusetts 02139

Laboratory experiments and numerical simulations have been conducted for plane channel flow with a streamwise-periodic array of cylinders. The primary transition in this open flow occurs as a convective rather than absolute instability and leads to traveling-wave packets, which advect out of the system. The ordered secondary state is characteristic of closed flows, in contrast with other open flows where the primary transition often leads directly to turbulence.

PACS numbers: 47.20.Ky, 47.20.Ft, 47.60.+i

The transition to turbulence has been most successfully described in closed fluid flows, such as flow between concentric rotating cylinders (Couette-Taylor flow), where fluid never advects out of the system. As a control parameter (e.g., Reynolds number R) is increased, a laminar closed flow typically becomes weakly turbulent only after the appearance of several intervening nonturbulent states, each of which is stable for a range of R and is spatially and temporally more complex than preceding states. This gradual progression toward turbulence has enabled detailed comparisons between theory and experiment.[1] In contrast, for open fluid flows, where fluid advects out of the system, connecting theory with experiment has been more difficult because these flows typically undergo a direct transition from laminar behavior to turbulence with complex spatial and temporal intermittency.[2] For example, in laminar plane channel flow, linear theory[3] predicts instability to two-dimensional traveling waves at a critical value of Reynolds number, $R_c = 5772.22$, while experiments[4] exhibit a subcritical (hysteretic) transition to turbulence for R as low as about 1000. Though nonlinear stability theory partially explains this behavior and numerical simulations suggest mechanisms for transition,[5] the primary-transition Reynolds number eludes prediction because of the high-dimensional nature of the secondary flow.

In this Letter, we present laboratory evidence for a supercritical (continuous) primary transition in a plane channel flow with spatially periodic geometrical perturbations. Our experiments and numerical simulations yield a value for R_c that is more than an order of magnitude smaller than for plane channel flow without perturbations. Previous numerical studies indicated that the reduction in R_c arises from destabilizing inflectional velocity profiles introduced by the perturbations and that the transition leads to two-dimensional traveling waves resembling the linear modes of the unperturbed case.[6] These waves, which grow from zero amplitude at R_c, are stable against two- and three-dimensional disturbances, unlike the unperturbed case where a subcritical transition leads to finite-amplitude modes that are stable to two-dimensional disturbances but unstable to three-dimensional disturbances.[7] Recent experimental heat-transfer studies[8] observed the onset of traveling waves near values of R_c predicted by numerical simulation, but no quantitative comparisons to hydrodynamic stability predictions were made. Further, these numerical and experimental studies did not distinguish between instabilities that are *absolute* (growing in time in any reference frame) or *convective* (growing in time only in a comoving frame); these concepts are important in understanding transitions in open and closed fluid flows.[9] We demonstrate that the supercritical primary transition arises from convective instability.

Figure 1 depicts a plane channel flow that is geometrically perturbed by an infinite number of cylinders in a spatially periodic array.[6,7] The channel half-depth h and the velocity U_0 are used to scale length, velocity, time t, and growth rate σ. U_0 is defined as $\frac{3}{2}$ times the streamwise velocity averaged in the cross-channel direction; in the unperturbed case U_0 is equal to the velocity at $y = 0$,
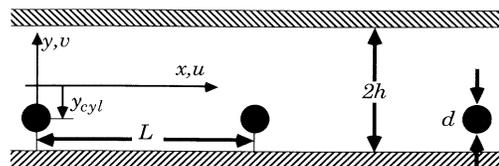

FIG. 1. Our geometry of plane channel flow with spatially periodic geometric perturbations, defined in units of the channel half-depth h by the streamwise cylinder spacing $L = 6.66$, the cross-channel cylinder location $y_{cyl} = -0.50$, and the cylinder diameter $d = 0.40$. The streamwise velocity is u and the cross-stream velocity is v. For the experiment, the spanwise dimension z (perpendicular to the figure) ranges from -20 to 20; the simulation is two dimensional.

but in the perturbed case this need not be true. The Reynolds number is defined as $R = U_0 h/v$, where v is the kinematic viscosity.

The experiment is performed in a water channel with $h = 0.794$ cm and with 21 cylinders, which approximate an infinite periodic array. Cylinder number 1 (numbering from upstream to downstream) lies a distance of 160 downstream from the channel inlet; the unperturbed flow approaches a parabolic profile in a length[10] $D \approx 0.11 U_0 h/v < 20$ for the range of R investigated. The experiment maintains constant-mass-flux inflow-outflow boundary conditions in x (streamwise). The fluid temperature is controlled to $\pm 0.1\,^\circ$C and the root-mean-square velocity fluctuation (noise) is typically 0.04% of U_0. Streamwise velocities u are measured by laser-Doppler and hot-film velocimeters; a separate laser-Doppler velocimeter measures U_0 at $x = -10.1$ upstream of cylinder number 1, $y = 0$, and $z = -5.1$.

The simulations are performed on a 32-processor Intel Hypercube using a spectral element spatial discretization.[11] Two cases of constant-mass-flux streamwise boundary conditions are considered: periodic with a single cylinder and inflow-outflow with nine cylinders. For the periodic calculations we impose $u(0,y) = u(L,y)$, $v(0,y) = v(L,y)$ for velocity and $p(0,y) = p(L,y)$ for pressure; a time-dependent body force corresponding to a mean pressure gradient maintains constant mass flux. For the inflow-outflow calculations, constant mass flux is specified by a parabolic velocity profile at the inflow; $du/dx = dv/dx = p = 0$ are maintained at the outflow.

In both the experiment and the simulation the primary transition is studied by intentionally disturbing the flow. In the experiment the disturbance in the mean velocity is a square pulse occurring everywhere down the channel with amplitude 0.3–0.6 and duration 2.5–4.5. The simulation starts from the equilibrium solution for the geometrically unperturbed flow; this initial condition causes spikes in velocity of amplitude ≈ 0.2. In both cases (Fig. 2), the initially broadband global disturbance evolves quite rapidly to a single oscillatory mode in time. This behavior holds for a range of R and suggests that the transition near R_c is a Hopf bifurcation,[12] where the modulus A_0 of the mode obeys the relation

$$dA_0/dt = \sigma A_0 - g A_0^3 , \qquad (1)$$

where $\sigma \sim \varepsilon \equiv (R - R_c)/R_c$.[13] (Since the geometry has no translational symmetry, there is no comoving frame where the transition can be viewed as a steady-state bifurcation.) For the range of ε considered here, we assume (1) to be valid without higher-order corrections and to correspond to a fixed wave number.

For R slightly less than R_c and A_0 small, the nonlinear term in (1) is neglected as t becomes large; $A_0(t)$ approaches $a_0 \exp(\sigma t)$. In the period after the broadband behavior of the disturbance (e.g., $t > 30$ for Fig. 2), velocity time series for several values of R are fitted by
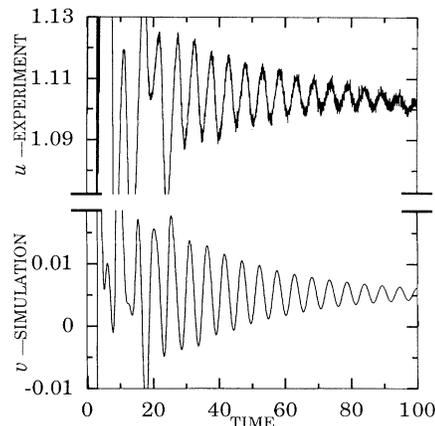

FIG. 2. Time series of fluid velocities in the laboratory experiment (top trace) and the numerical simulation (bottom trace) for similar subcritical values of R. Streamwise velocity u in the experiment was measured by a laser-Doppler velocimeter at $x = 3.9$ downstream of cylinder number 18, $y = 0$, and $z = -5.1$ for $R = 110.5$. Cross-stream velocity v in the simulation with streamwise-periodic boundary conditions was recorded at $x = 1.6666$ and $y = y_{\text{cyl}} = -0.5$ for $R = 115.0$. All quantities are dimensionless—see text.

$b + a_0 \exp(\sigma t) \sin(\omega t + \phi)$ with b, a_0, σ, ω, and ϕ as free parameters. Extrapolating a linear regression fit of σ vs R to zero growth rate, we estimate $R_c = 128.5 \pm 0.3$ for the experiment and $R_c = 136.0 \pm 0.6$ for the simulation [Fig. 3(a)]. The error bounds indicate the precision of R_c, but possible systematic errors limit the accuracy of the R_c values to $\pm 5\%$.

For R slightly greater than R_c, a single mode still evolves from the initial broadband behavior, but the modulus of the mode increases and approaches a limiting value, as in a supercritical Hopf bifurcation [$g > 0$ in (1)]. With $dA_0/dt = 0$ in the long-time limit of (1), the nonlinear saturation of A_0 scales as $\varepsilon^{1/2}$. Furthermore, the nonlinear self-interaction of A_0 generates harmonics A_n that scale as $\varepsilon^{(n+1)/2}$ for small ε. For several values of R, velocity time series in the period where the single mode was saturated are fitted by

$$b + A_0 \sin(\omega t + \phi_0) + A_1 \sin(2\omega t + \phi_1) ,$$

with b, A_0, A_1, ω, ϕ_0, and ϕ_1 as free parameters. With $R_c = 128.5$ for the experiment and $R_c = 136.0$ for the simulation, linear regression fits of A_0 and A_1 vs ε yield exponent estimates of 0.53 ± 0.01 for A_0 and 1.00 ± 0.02 for A_1 in the experiment, 0.59 ± 0.05 for A_0 and 1.1 ± 0.1 for A_1 in the simulation [Fig. 3(b)]; the error bounds of A_0 and A_1 were found by varying R_c by ± 1 standard deviation and repeating the linear regression analysis.

In Fig. 4 simultaneous velocity data at two spatial points in the experiment illustrate that the transition arises from convective instability. Initially both time
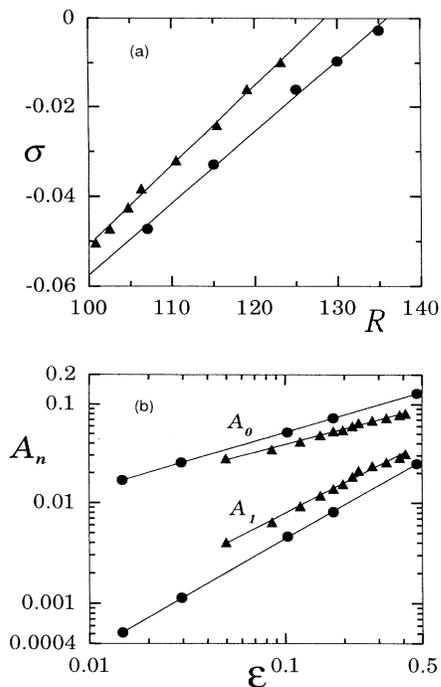
FIG. 3. (a) Growth rates σ below transition and (b) saturation amplitudes of the first two Fourier components, A_0 and A_1, above transition are compared for u from the experiment at $x = 3.9$ downstream of cylinder number 18, $y = 0$, and $z = -5.1$ (▲) and for v from the simulation (streamwise-periodic boundary conditions) at $x = 1.6666$ and $y = -0.5$ (●).
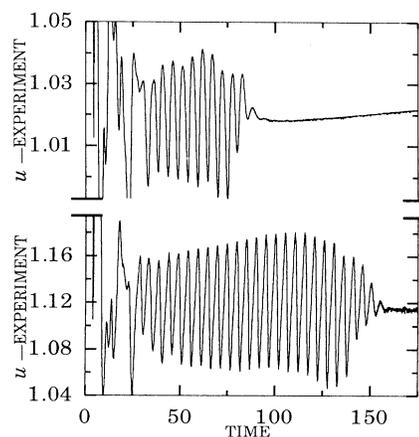

FIG. 4. The convective nature of the transition observed in the experiment is illustrated by these simultaneous measurements of velocity at two spatial points for $R = 151.2$. The upper trace was recorded from a hot-film velocimeter at $x = 2.4$ downstream of cylinder number 10, $y = 0$, and $z = 16.8$, and the lower trace was recorded from a laser-Doppler velocimeter at $x = 3.9$ downstream of cylinder number 18, $y = 0$, and $z = -5.1$.

series evolve similarly; however, after some time, u at the upstream probe (top trace, Fig. 4) becomes steady while u at the downstream probe (bottom trace, Fig. 4) continues to grow. Eventually, u at the downstream probe also becomes steady as the tail of the wave packet advects past the downstream probe and out of the experiment. The wave packet's time of flight through the experiment limits the observation time for growth rates with $\varepsilon < 0$ and for saturation amplitudes with $\varepsilon > 0$. Without imposed disturbances we first observe unsteadiness in the form of weak intermittent oscillations for R well above R_c; studies of models[14] with convective instabilities suggest that these oscillations are triggered by background noise.

Simulations are conducted with streamwise-periodic boundary conditions to model the primary transition using (1); however, since periodicity prevents distinguishing between absolute and convective instability, simulations are also conducted with streamwise inflow-outflow boundary conditions (Fig. 5). As in the experiment, the initial disturbance rapidly evolves into a wave packet consisting of two waves per rod spacing and subsequently advects out of the flow domain. Despite the different boundary conditions for the two types of simulations, a direct comparison of the flow fields starting from the

same initial conditions demonstrates that a velocity time series at a given point in space evolves identically in time until the wave-packet tail, whose width in time is $\sim D/U_0$, advects past the inflow-outflow simulation.

The present work demonstrates the relevance of supercritical nonlinear models like (1) to transitions arising from a convective instability in a channel flow. Previous experiments[2] in open flow past a single cylinder have shown the primary transition in that system is a Hopf bi-
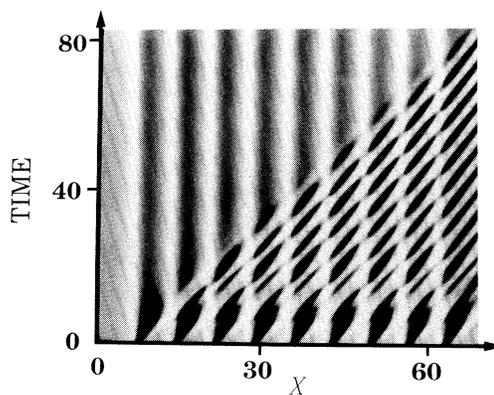

FIG. 5. Transition arising from a convective instability in the simulation with nine cylinders and inflow-outflow streamwise boundary conditions is illustrated by a plot of v at 200 evenly spaced x locations with $y = 0.395$ for 162 consecutive time intervals at $R = 160$. The lightest regions indicate the largest velocities. The streamwise locations of the cylinders (light bands parallel to the time axis) are indicated by the x dependence of the steady v due to flow past the cylinders.

furcation; however, the resulting von Kármán vortex street is governed by an absolute instability in the near wake.[15] In addition, in flow past a cylinder the Strouhal number (oscillation frequency scaled by a velocity and a length) shows a strong dependence on R near R_c with $\varepsilon > 0$.[16] In contrast, the Strouhal number in our study is 0.195 ± 0.002 for the experiment and 0.188 ± 0.001 for the simulation, nearly independent of R and in reasonable agreement with the Strouhal number from linear theory for the geometrically unperturbed case (0.180 at $R = 130$).[6,17] Future investigation of the ordered secondary flow should include the study of bifurcations to higher instabilities and to turbulence. Connections between dynamical systems theory and transitions in the unperturbed case may be revealed by varying the geometrical parameters that define the spatially periodic perturbations in this problem.[18]

[a]Present address: Department of Physics, Campus Box 172, University of Colorado–Denver Campus, Denver, CO 80217.

[b]Present address: Center for Research on Parallel Computation, California Institute of Technology, Pasadena, CA 91125.

[1]P. Manneville, *Dissipative Structures and Weak Turbulence* (Academic, San Diego, 1990).

[2]Open flows that are exceptions include the following: flow past a cylinder, e.g., C. Mathis, M. Provensal, and L. Boyer, J. Phys. (Paris), Lett. **45**, 483 (1984), and Rayleigh-Bénard or Couette-Taylor systems subject to a mean throughflow, e.g., H. W. Müller, M. Lücke, and M. Kamps, Europhys. Lett. **10**, 451 (1989).

[3]S. A. Orszag, J. Fluid Mech. **50**, 689 (1971).

[4]M. Nishioka and M. Asai, J. Fluid. Mech. **150**, 441 (1985).

[5]W. C. Reynolds and M. C. Potter, J. Fluid Mech. **27**, 465 (1967); S. A. Orszag and A. T. Patera, J. Fluid Mech. **128**, 347 (1983).

[6]G. E. Karniadakis, B. B. Mikic, and A. T. Patera, J. Fluid Mech. **192**, 365 (1988).

[7]C. H. Amon and A. T. Patera, Phys. Fluids A **1**, 2005 (1989); G. E. Karniadakis and C. H. Amon, in *Proceedings of the Sixth IMACS International Symposium on Partial Differential Equations,* edited by R. Vichnevetsky and R. S. Stepleman (International Association of Mathematics and Computers in Simulation, New Brunswick, NJ, 1987), p. 525.

[8]H. Kozlu, Ph.D. thesis, MIT, 1989 (unpublished); M. Greiner, R. F. Chen, and R. A. Wirtz, ASME J. Heat Transfer **112**, 336 (1990).

[9]R. J. Deissler, Phys. Fluids **30**, 2303 (1987); P. Huerre and P. A. Monkewitz, Annu. Rev. Fluid Mech. **22**, 473 (1990); R. P. Tagg, W. S. Edwards, and H. L. Swinney, Phys. Rev. A **42**, 831 (1990).

[10]H. Schlichting, *Boundary Layer Theory* (McGraw-Hill, New York, 1968), 6th ed.

[11]P. F. Fischer and A. T. Patera, J. Comput. Phys. (to be published).

[12]J. Guckenheimer and P. Holmes, *Nonlinear Oscillations, Dynamical Systems, and Bifurcations of Vector Fields* (Springer-Verlag, New York, 1983).

[13]More generally, (1) would also include spatial gradient terms (the Ginzburg-Landau equation). Since we measure amplitudes in the center of evolved wave packets, where spatial variation is small, we omit such terms in (1).

[14]R. J. Deissler, Physica (Amsterdam) **25D**, 233 (1987).

[15]G. S. Triantafyllou, K. Kupfer, and A. Bers, Phys. Rev. Lett. **59**, 1914 (1987).

[16]J. H. Gerrard, Philos. Trans. Roy. Soc. London A **288**, 351 (1978).

[17]W. S. Edwards (private communication).
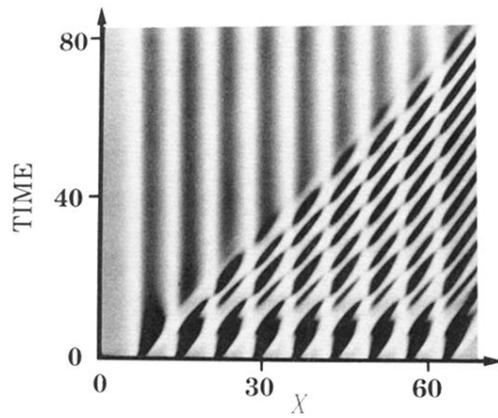
[18]D. Barkley, Phys. Fluids A **2**, 955 (1990).

FIG. 5. Transition arising from a convective instability in the simulation with nine cylinders and inflow-outflow streamwise boundary conditions is illustrated by a plot of v at 200 evenly spaced x locations with $y = 0.395$ for 162 consecutive time intervals at $R = 160$. The lightest regions indicate the largest velocities. The streamwise locations of the cylinders (light bands parallel to the time axis) are indicated by the x dependence of the steady v due to flow past the cylinders.